Three-dimensional evolution of ensemble forecast spread during the onset of a stratospheric sudden warming event in January 2006

Kazuaki NISHII*, Hisashi NAKAMURA

Department of Earth and Planetary Science, Graduate School of Science, The University of Tokyo, Japan.

Abstract: Analysing the evolution of ensemble forecast spread, which represents the growth of errors in the initial field and therefore uncertainty of forecasts for subsequent fields, is useful for identifying particular circulation features that can impact the forecast skill of a subsequent phenomenon of interest. In this study, the trigger of a major stratospheric sudden warming (SSW) event observed in late January is investigated by applying a singular value decomposition analysis and a simple sensitivity analysis to the spread of a set of operational long-range ensemble forecasts. The analyses show that the predictability of the SSW event is particularly sensitive to uncertainty in the initial state in the vicinity of a developing synoptic-scale cyclone that was observed over the North Pacific more than two weeks prior to the peak of the event. A local maximum of initial errors identified around the cyclone grows in time as the forecast errors increase. After its translation in correlation with observed downstream development of synoptic-scale disturbances, the spread maximum reaches the subpolar North Atlantic, where a blocking ridge is observed to develop as the source of an upward-propagating Rossby wave packet that gives rise to the deceleration of the stratospheric polar-night jet (PNJ). The largest forecast errors then extend upward with the wave packet, causing pronounced uncertainty in the predicted strength of the PNJ deceleration. The present study suggests the Pacific cyclone as an important trigger of the prominent SSW event, confirming the importance of the key dynamical processes discussed above that caused the event.

1 Introduction

During a stratospheric sudden warming (SSW) event, the stratospheric polar vortex warms up by several tens of degrees. A westerly polar-night jet (PNJ) concomitantly weakens and, in prominent events, reverses its direction within a few days. It is now established that SSW events, regarded also as manifestations of extreme negative events of the stratospheric Northern Annular Mode (NAM), act to turn the phase of the tropospheric NAM into negative (Baldwin and Dunkerton, 1999, 2001; Limpasuvan *et al.* 2004). Thus forecast errors of an SSW event may impact the forecast skill of the subsequent evolution of

*Correspondence to: Department of Earth and Planetary Science, Graduate School of Science, The University of Tokyo, Tokyo, 113-0033, Japan. E-mail: nishii@eps.s.u-tokyo.ac.jp

Prepared using qjrms3.cls [Version: 2007/01/05 v1.00]

the tropospheric circulation, as suggested by ensemble forecast experiments by Charlton *et al.* (2004, 2005) and by Mukougawa and Hirooka (2008).

An SSW event has been shown to occur due to anomalous amplification of upward planetary waves from the troposphere (*e.g.,* Matsuno 1971). In order to examine how the forecast skill of SSW events depends on the tropospheric circulation, a series of studies has recently been conducted by using operational ensemble forecasts produced by the Japan Meteorological Agency (JMA). For example, Mukougawa *et al.* (2005) have shown that the formation of a blocking ridge over the North Atlantic was important for the enhancement of upward propagation of planetary-wave activity into the stratosphere and the warming of the polar stratosphere observed in December 2001. Mukougawa *et al.* (2007) have confirmed the above result through hindcast experiments with initial conditions in which the observed blocking flow configuration was artificially perturbed. The JMA ensemble forecast products were also used for examining the predictability of other prominent SSW events (Mukougawa and Hirooka, 2004; Hirooka *et al.* 2007).

In this paper, we present a case study on the predictability of a major SSW event observed in January 2006 (Manney *et al.* 2008). Prior to this event, the zonal-mean PNJ had gradually weakened from late December 2005. This weakening associated with several events of enhanced upward propagation of planetary-wave activity from the troposphere. Nishii *et al.* (2009; hereafter NNM09) have found that those events were contributed to significantly by zonally-confined Rossby wave packets propagating into the stratosphere from tropospheric quasi-stationary circulation anomalies. In one of these events that occurred just before the PNJ had become easterly in mid-January, a Rossby wave packet that emanated

from a tropospheric anticyclonic circulation anomaly over the subpolar North Atlantic was found to be the primary contributor to the enhanced injection of planetary-wave activity into the stratosphere. The tropospheric anticyclonic anomaly amplified due to anomalous vorticity flux divergence associated with synoptic-scale transient eddies along the Atlantic storm track. Their intensification over the Atlantic was found to follow the downstream development of synoptic disturbances from the North Pacific.

The aim of this study is to analyse the growth of initial errors in the individual members of the JMA operational ensemble forecasts over the two weeks prior to the particular SSW event. By tracing the three-dimensional evolution of the ensemble forecast spread and conducting a singular value decomposition (SVD) analysis and a simple sensitivity analysis for the ensemble members, we show that the large ensemble spread in the intensity of the stratospheric PNJ predicted in the SSW event arises largely from the forecast spread in the Rossby wave packet emanating upward from the tropospheric anticyclonic anomaly over the Atlantic. We also show that the prediction skill of the anticyclonic anomaly is particularly sensitive to initial errors around the synoptic-scale cyclone developing over the North Pacific about two weeks before the peak of the SSW event. We confirm these relatively large analysis errors around the particular cyclone by investigating an experimental reanalysis data set that includes information on the accuracy of the analysis.

2 Data

The ensemble forecast product utilized in this study was produced by the JMA Operational Monthly Forecast System (JMA, 2002). Resolution of the forecast model is

T106L40. The model has 13 vertical levels above the 100-hPa level, and the model top is placed at the 0.4-hPa level. Initial perturbation fields were constructed through a combination of the Breeding of Growing Modes (BGM) method (Toth and Kalnay, 1993) and the Lagged Average Forecasting (LAF) method (Hoffman and Kalnay, 1983). Routine forecasts are performed every Wednesday and Thursday. We use a particular set of the JMA forecasts with their initial fields for 11 or 12 January 2006. For each of the initial dates, six different ("positive") perturbation fields were generated by the BGM method. The ensemble members were doubled by adding the same perturbation fields but with their polarity reversed ("negative"). With the unperturbed initial field included, the total number of the ensemble members is thus 13 for each of the initial dates. Unless otherwise noted, the ensemble members initialized on 11 and 12 January are combined together in our analysis. This is because the members started on 11 January can be regarded as if they were initiated on 12 January, with initial perturbations developing from those for 11 January. This interpretation is consistent with the basic idea of the LAF method. Forecast spread among the ensemble members is regarded as a measure of uncertainty in the forecasted fields. The spread is defined at each grid point as the variance of a particular variable among the ensemble members about its ensemble mean.

Observational fields for the verification have been provided by the JMA Climate Data Assimilation System (JCDAS), as a continuation from the Japanese 25-year Reanalysis (JRA-25; Onogi *et al.* 2007). The ensemble prediction system operated around the SSW event considered in this study used the same forecast model as in the JRA-25 assimilation system, which is reported to have a cold bias in the lower and middle stratosphere (Onogi *et al.* 2007). While a cold bias in the assimilation system does not emerge in the JRA-25 and JCDAS data as long as observational data are available in the stratosphere, the ensemble forecasts may suffer from such a bias in a significant manner.

3 Uncertainty in the predicted PNJ

Figure 1(a) shows a time series of 20-hPa zonal-mean zonal wind velocity for the individual ensemble forecast members operated by the JMA with their initial conditions taken from the observations on 11 or 12 January 2006 (red and blue lines). The spread of the predicted wind velocity among the members increases rapidly with time in the period between 21 and 28 January, during which the observed 20-hPa PNJ (a dashed black line) underwent the most rapid deceleration during the SSW event. Correspondingly, the forecast spread is also large in the zonally-averaged meridional eddy heat flux at the 100-hPa level (Figure 1(b)). The heat flux is equivalent to a vertical component of the Eliassen and Palm (E-P) flux based on the quasi-geostrophic, beta-plane formulation (Andrews *et al.* 1987). The flux can therefore be regarded as a measure of the upward injection of planetary-wave activity from the troposphere that caused the PNJ deceleration. Many of the members can predict the amplification of the flux until around 17 January. Although the observed heat flux remains as large as 20 K m s^{-1} for the next several days, most of the ensemble members apparently underestimate the flux, especially after 20 January. Presumably this underestimation causes the misforecast of the PNJ deceleration after 21 January in most of the ensemble members. One may notice that the heat flux predicted in several ensemble members is greater than its observational counterpart (Figure 1(b)), but these members nevertheless underestimate the PNJ deceleration (Figure 1(a)). As will be discussed later, this could be due to the stratospheric

cold bias in the numerical model used for the JMA ensemble forecasts we analyse in this study.

4   Three-dimensional evolution of the forecast spread

On 16 January, just before the onset of the rapid PNJ deceleration (Figure 1(a)), the lower-stratospheric polar vortex had already been weakened and split (Figure 2(a)). In fact, anticyclonic anomalies at the 50-hPa level were observed over the Arctic and the North American continent (contoured in Figure 2(d)). Here, anomalies are defined as local deviations from the climatology defined for each calendar day based on the JRA-25 data for the period 1980-2003. Shading in Figure 2(d) indicates the horizontal distribution of the ensemble forecast spread for 16 January in the lower stratosphere. Because its magnitude increases with time, the local spread for a given forecast day has been normalized by its instantaneous maximum within the domain (poleward of 20°N). It is apparent in Figure 2(d) that the large spread is confined to the subpolar North Atlantic. Although the area of the large forecast spread in 50-hPa height gradually expands horizontally, the spread maximises over the subpolar North Atlantic throughout the period of the rapid PNJ deceleration from 20 to 28 January (Figures 2(e) and 2(f)). As shaded in Figure 3, the ensemble forecast spread over the North Atlantic and Europe (60°W-60°E) undergoes upward extension from the troposphere into the stratosphere at the onset stage of the PNJ deceleration (note that the spread and anomaly are normalized by the pressure in the figure). On 16 January (Figure 3(a)), the particularly large spread (plotted with heavy shading) is confined to the vicinity of a tropospheric anticyclonic anomaly around 40°W associated with a prominent blocking flow configuration over the North Atlantic (Figure 4(b)). The anomaly

acted as the source of the Rossby wave packet that propagated into the stratosphere (NNM09). In fact, as the tropospheric anticyclonic anomaly weakened, the stratospheric cyclonic anomaly over western Europe (around the Greenwich Meridian) amplified with their phase lines tilting westward with height (Figures 3(a) and 3(b)). These features are indicative of upward group velocity propagation of a Rossby wave packet. Interestingly, unlike in the troposphere, the ensemble spread in the stratosphere is not maximised near the centre of the cyclonic anomaly at each level. Rather, it is maximised around node lines of the height anomalies on the upstream and downstream side of the centre (Figures 3(b) and 3(c)). Furthermore, the cyclonic anomaly centre over Europe for each of the ensemble members, which is defined as the strongest negative deviation of 50-hPa height from the observed climatology and plotted with a black dot in Figures 2(d) and 2(e), tends to displace farther from the observed cyclonic anomaly centre, as the forecast spread extends upward into the stratosphere (from 16th to 20th of January). We thus conjecture that the forecast spread extends into the stratosphere in correlation with the Rossby wave packet that contributed to the SSW event, probably reflecting inconsistencies in its magnitude, group velocity and/or wavelengths simulated among the ensemble members. In fact, Figure 1(b) indicates that as the forecast spread extends into the stratosphere after 16 January, underestimation of the wave-activity injection into the stratosphere becomes apparent in many of the ensemble members.

As NNM09 pointed out, the tropospheric blocking ridge and associated anticyclonic anomaly over the subpolar North Atlantic (Figures 4(b) and 4(d)), from which the ensemble spread extends into the stratosphere (Figure 3), developed by 16 January in association with downstream development of synoptic-scale disturbances from

the North Pacific into the North Atlantic. The downstream development can be confirmed in 250-hPa geopotential height and squared meridional wind fields shown in Figures 5. The height contours over the Pacific were almost zonal on 11 January (Figures 5(a)). The wave packet associated with meandering westerlies emerged on 12 January over the central Pacific and then propagated downstream until blocked by the developing anticyclonic ridge over the Atlantic around 15 January. Observed maxima of the squared 250-hPa meridional wind velocity associated with this wave packet (Figure 5(b)) exhibit a signature of group velocity propagation across the North Pacific and Atlantic from 12 to 16 January. As indicated in Figure 5, crude estimations of the group velocity (rectangle with solid line) and phase speed (dashed line) based on Figure 5(b) are about $31°$ and $7°$ in longitude per day, respectively. The former appears to correspond to the zonal group velocity of a baroclinic wave packet (Chang 1993), while the latter is in agreement with typical zonal phase speed of synoptic-scale baroclinic waves (Wallace *et al.* 1988).

Downstream extension of the ensemble forecast spread maximum in the troposphere has been reported by Anwender *et al.* (2008) and Harr *et al.* (2008). This extension is also observed in our analysis associated with the downstream development of migratory synoptic-scale disturbances. In fact, the local maximum of the ensemble spread in 250-hPa meridional wind velocity appears to translate zonally across the Northeastern Pacific rather slowly (about $8°$ per day; dashed line in Figure 5(c)). In addition, the downstream extension of the large forecast spread is suggested, as indicated by a rectangle with a solid line in Figure 5(c). The speed of this downstream extension into the Atlantic is about $26°$ in longitude per day, which is similar to but slightly slower than the group

velocity of the observed wave packet as estimated in Figure 5(b). Eastward translation of forecast errors across the North American continent associated with the downstream development of synoptic-scale disturbances has been reported by Langland *et al.* (2002). In the case they analysed, the eastward propagation of the errors was faster than the phase speed of synoptic-scale troughs and ridges and slightly slower than a wave-packet propagation, consistent with our analysis. Our analysis is also consistent with the result of Rabier *et al.* (1996), who showed that forecast errors propagate downstream from the North Pacific or North America as far as into Europe in a comparison of forecasts started from routinely constructed analyses with those from initial values improved by the adjoint method.

On 12 January, one of the initial dates for the ensemble forecasts we analysed, local maxima of the ensemble spread in 250-hPa geopotential height are found not only over the North Pacific but also over North Africa and South Asia (Figure 4(c)). However, the growth of any of the latter two spread maxima is less than that of the North Pacific maximum located just downstream of the particular cyclone that appears to be the origin of the "downstream development" of the ensemble spread. The corresponding spread maximum is also observed in SLP over the North Pacific around the particular surface cyclone (not shown).

In this section, we have traced the evolution of the spread maximum. The spread maximum first appeared as initial errors around the Pacific cyclone, then translated in correlation with the observed downstream development from the Pacific as far as the Atlantic blocking high. Finally, the spread maximum propagated into the stratosphere in association with the observed Rossby wave packet emanated from the blocking high, resulting in the

forecast errors of the SSW event.

5 Cluster analysis among the ensemble members

The "group-velocity propagation" of the forecast spread shown in the preceding section (Figure 5(c)) may represent inconsistency among the ensemble members in phase and/or amplitude of eddy components developing downstream. To confirm this, a cluster analysis based on the Ward method (Ward, 1963) was applied to 250-hPa geopotential height over the Pacific predicted by the ensemble members for 14 January (Figure 1(c)). The analysis domain is (180°-300°E and 20°N-60°N), and pattern proximity between a pair of clusters is measured by Euclidean distance.

After several trials, we found the ensemble members to be categorized into two clusters, one (Cluster A) characterized by relatively fast phase speed and small amplitudes of synoptic-scale disturbances (red contours in Figure 1(c)), and the other (Cluster B) by their slower phase speed and larger amplitudes (blue contours). It is noteworthy that in Cluster A, the blocking high over the North Atlantic, which is regarded as the source for the upward-propagating wave packet (Figures 3 and 4(b)), tends to develop more strongly with more pronounced poleward meanders of the westerlies than in Cluster B and in the observations as well (Figure 1(d)). This feature is particularly obvious in 2 members of Cluster A for which the PNJ deceleration is successfully predicted (red heavy dashed lines in Figure 1(a)) and the tropospheric westerlies are predicted with pronounced poleward meanders over the Atlantic (red heavy dashed contours in Figure 1(d)). These two members predict the upward wave-activity flux that is stronger than in the observations (Figure 1(b)), although the predicted PNJ deceleration is nevertheless comparable to the observations (Figure 1(a)). The fact that the ensemble members that predict realistic PNJ deceleration tend to overestimate the blocking intensity in the JMA forecast model suggests that unrealistically strong upward flux of planetary-wave activity may be necessary in the forecast model for decelerating the PNJ as much as in the real atmosphere associated with the SSW event. This may be due to the cold bias in the forecast model (Onogi *et al.* 2007), which can introduce an artificial tendency for stratospheric temperatures to resist against the warming induced by incoming planetary waves from the troposphere. These results imply that mechanisms for the amplification and propagation of the planetary waves in ensemble members that predict an SSW event successfully may not necessarily be the same as in the real atmosphere, if the forecast model has a non-negligible bias.

6 SVD analysis

A singular value decomposition (SVD) analysis was applied to all the 26 ensemble forecast members, in order to confirm the relationship between the development of the Atlantic anticyclonic anomaly (Figure 4(b)) and initial errors or other forecasted fields. An SVD analysis is often applied to time-varying fields of two variables, in order to extract their dominant co-variability based on their temporal covariance matrix (Bretherton *et al.* 1992). In our application, SVD is applied to a matrix whose element is the covariance between deviations of a given variable among the 26 members from its ensemble mean at a given location for a particular forecast time and the corresponding deviations of any variable at any location for any forecast time. In each of our applications, every field has been normalized by its standard deviation among the ensemble members, and therefore the matrix is eventually a cross-correlation matrix. We focus on the leading SVD mode that has the largest singular value and therefore explains

the largest fraction (more than 40% in our applications) of their spatially-integrated squared covariance.

A set of SVD analyses was performed between the ensemble of 250-hPa geopotential height fields forecasted for 16 January over the subpolar North Atlantic (270°E-357.5°E, 40°N-85°N), where the prominent blocking was observed, and the same or other forecasted fields over the entire extratropical northern hemisphere (northward of 20°N). Each panel of Figure 6 shows a hemispheric map of the heterogeneous regression coefficient of a given variable for a particular forecast time calculated with the normalized expansion coefficients of the first SVD mode for the 26 members of the 250-hPa height over the North Atlantic forecasted for 16 January. In each of the panels (a), (b), (d) and (e), we can identify regions where the forecast spread or initial error is strongly related to the spread of the blocking signature over the subpolar North Atlantic forecasted for 16 January. In panels (f) and (g) of Figure 6, we can also identify regions where the spread of the blocking signature forecasted for 16 January influences the forecast spread at a later forecast time most sensitively. The corresponding heterogeneous regression map (Figure 6(c)) of 250-hPa height forecasted over the North Atlantic for 16 January with the expansion coefficients of the first SVD mode represents uncertainty in the forecasted intensities of the blocking and concomitant upstream wave signal.

Figure 6(a) indicates that the large forecast spread in 250-hPa height over the North Atlantic for 16 January is particularly sensitive to initial errors in 250-hPa height over the North Pacific on 12 January. Specifically, a positive signal in Figure 6(a) is located slightly upstream of an anticyclonic ridge observed near the date line and downstream of the pressure trough that has been identified as the origin of the downstream development of synoptic

disturbances (Figures 5(a) and 5(b)). The corresponding maximum sensitivity in 1000-hPa geopotential height on 12 January is located over the central North Pacific (Figure 6(d)). Again, this positive signal is located slightly upstream of a surface pressure ridge and downstream of the surface cyclone, as represented by heavy solid and dashed contours, respectively, in Figure 6(d).

This SVD result indicates that the synoptic-scale cyclone over the North Pacific is one of those circulation systems in the initial state to which the amplification of the North Atlantic blocking ridge in the forecast for 16 January is most sensitive. More specifically, the positive height signal just upstream of the pressure ridge suggests that the synoptic wave packet that consists of the pressure ridge and trough over the North Pacific tends to be shorter in zonal wave length for the ensemble members with stronger development of the North Atlantic blocking on 16 January, and vice versa. A wave packet with shorter wave length tends to accompany stronger fluctuations in meridional wind velocity and thus the stronger zonal component of a wave-activity flux than that with longer wave length. In fact, the corresponding positive signal of 250-hPa meridional wind is found over the observed southerlies over the North Pacific (Figure 6(e)). The enhanced meridional wind velocity yields stronger downstream development across the Pacific and North America, which can lead to enhanced development of the Atlantic blocking.

The same SVD analysis as above but for the hemispheric field of 250-hPa height forecasted for 14 January (Figure 6(b)) reveals that significant positive and negative signals of geopotential height along the east coast of North America forecasted for 14 January are sensitively related to the strength of the North Atlantic blocking

forecasted for 16 January. These positive and negative signals are located slightly upstream and downstream of an observed pressure trough off the east coast of Canada. A comparison with Figure 1(c) indicates that these signals are a manifestation of the sensitivity of the blocking ridge development to the longitudinal position of the pressure trough to its upstream that constitutes the wave packet propagating from the Pacific.

The same SVD analysis with the forecasted 250-hPa height over the subpolar North Atlantic was also applied to the upward fluxes of Rossby wave activity (Plumb, 1985) evaluated for 18 January at the 100-hPa level based on the individual forecast members (Figure 6(f)). The analysis indicates that the wave-activity flux into the stratosphere from the tropospheric anticyclonic anomaly over the North Atlantic tends to increase with the amplitude of the anomaly (Figure 6(f)). Taking it into consideration that the upward wave-activity flux formulated by Plumb (1985), if zonally averaged, is equivalent to the upward E-P flux, this result is in agreement with the tendency observed in Figure 1 that the stronger meander of the tropospheric westerlies over the North Atlantic is more favorable for the stronger upward wave-activity propagation into the stratosphere. Our SVD analysis further demonstrates that large forecast spread in 50-hPa height over the North Atlantic for 20 January (Figure 2(e)) is most sensitive to the amplitude of the tropospheric blocking ridge forecasted a few days earlier (Figure 6(g)), in a manner consistent with its sensitivity to the magnitude of the upward wave-activity flux (Figure 6(f)). The strongest sensitivity and maximum forecast spread in 50-hPa height for 20 January are identified around the node of the circulation anomalies actually observed (Figure 2(e)), suggesting that the large uncertainty in the position of the 50-hPa cyclonic anomaly centre among the ensemble members

for 20 January (Figure 2(e)) arises probably from the forecast errors in the strength of the tropospheric blocking ridge over the North Atlantic. Our SVD analysis shown in Figures 6(a-g) has revealed the relationship between forecast spread in the intensity of the blocking ridge over the North Atlantic on 16 January and that in other fields on the days before and after 16 January. The co-variability of the leading SVD mode for each of the pairs explains more than 40% of the total covariance squared.

Finally, a similar SVD analysis was applied to hemispheric fields between 250-hPa height on 12 January and 50-hPa height on 28 January, when the observed PNJ was most strongly westward (Figure 1(a)). In a heterogeneous regression map (Figure 6(h)), a positive signal in 250-hPa height is again found for 12 January over the North Pacific, as in Figure 6(a) but slightly downstream. The co-variability of the particular leading mode, however, explains only 24% of the total covariance, because of the weaker correlation between the two fields reflecting the longer lead time.

7 Simple sensitivity analysis

To substantiate the aforementioned results further, we have conducted a simple sensitivity analysis as introduced by Enomoto *et al.* (2006, 2007). The analysis utilizes a result of an ensemble forecast to identify initial perturbations that can grow optimally into a given verification region over a given forecast period. We first give a brief explanation of the analysis, following Enomoto *et al.* (2006).

Suppose that time evolution of the i-th ensemble member ($i = 1, 2, \cdots, m$) may be expressed as

$$\mathbf{z}_i = M\mathbf{y}_i, \qquad (1)$$

where $\mathbf{y}_i$ and $\mathbf{z}_i$ are initial and forecasted perturbations, respectively, and M denotes a mapping operator. Note that the perturbations here are defined as deviations from the unperturbed member but not from the ensemble average. With matrices Y and Z that consist of $\mathbf{y}_i$ and $\mathbf{z}_i$, respectively, as their columns, linear combinations of the initial and forecasted perturbations can be expressed as

$$\mathbf{y} = p_1\mathbf{y}_1 + p_2\mathbf{y}_2 + \cdots + p_m\mathbf{y}_m = Y\mathbf{p} \qquad (2)$$

and

$$\mathbf{z} = p_1\mathbf{z}_1 + p_2\mathbf{z}_2 + \cdots + p_m\mathbf{z}_m = Z\mathbf{p}, \qquad (3)$$

respectively, with a vector $\mathbf{p}$ that consists of the coefficients p_i. Then one can find a particular $\mathbf{p}$ that maximises the norm of $\mathbf{z}$ ($\|\mathbf{z}\|$) in the verification region under the constraint that the norm of $\mathbf{y}$ ($\|\mathbf{y}\|$) equals to unity. Here, $\|\mathbf{y}\|^2$ and $\|\mathbf{z}\|^2$ are defined as

$$\|\mathbf{y}\|^2 = <\mathbf{y}^T, G\mathbf{y}> = \mathbf{p}^T Y^T G Y \mathbf{p}, \qquad (4)$$

and

$$\|\mathbf{z}\|^2 = <\mathbf{z}^T, H\mathbf{z}> = \mathbf{p}^T Z^T H Z \mathbf{p}, \qquad (5)$$

where G and H are positive definite symmetric matrices. In our application, the norm of an arbitrary perturbation $\mathbf{x}$ is defined in terms of dry total energy as

$$
\begin{aligned}
\|\mathbf{x}\|^2 &= \quad <\mathbf{x}^T, F\mathbf{x}> \\
&= \quad \frac{1}{2}\iint_A \{u'^2 + v'^2 \\
&\quad + \frac{C_p}{T_r}T'^2 + RT_r(\frac{p_s'}{p_r})^2\}dAdp, \qquad (6)
\end{aligned}
$$

where u', v', T' and p_s' denote perturbations in the zonal and meridional wind velocities, temperature and surface pressure, respectively. In Equation (6), C_p and R denote the specific heat at constant pressure and the gas constant,

respectively, of dry air, T_r and p_r signify the reference values of temperature and pressure, respectively, at the surface, A denotes the area of the domain specified for analysis, and F is an operator that symbolically represents the particular energy norm defined for the domain. In our analysis, the operator matrix G in Equation (4) was chosen in such a manner that dry total energy of the initial perturbations was integrated horizontally over the northern hemisphere poleward of 30°N and vertically between the 1000- and 100-hPa levels for each of the initial dates of the forecast (11 or 12 January). Likewise, the operator H was defined for expressing the dry total energy of the forecast field over a given verification domain as specified below.

To find $\mathbf{p}$ that maximises $\|\mathbf{z}\|^2$, the Lagrange multiplier method was used for finding extrema of the following function,

$$f(\mathbf{y}, \lambda) = \mathbf{p}^T Z^T H Z \mathbf{p} - \lambda(\mathbf{p}^T Y^T G Y \mathbf{p} - 1). \quad (7)$$

Since H and G are symmetric, differentiating f with respect to $\mathbf{p}$:

$$\frac{\partial f(\mathbf{y}, \lambda)}{\partial \mathbf{p}} = 2(Z^T H Z \mathbf{p} - \lambda Y^T G Y \mathbf{p}) = \mathbf{0} \qquad (8)$$

leads to a generalized eigenvalue problem

$$Z^T H Z \mathbf{p} = \lambda Y^T G Y \mathbf{p}. \qquad (9)$$

By substituting $\mathbf{p}$ as obtained as a solution of Equation (9) into Equation (2), we can identify initial perturbations that will evolve into the most developed perturbation over the given forecast within the verification domain. We used only the first eigenvector for each of our analysis as discussed below, whose eigenvalue accounts for nearly 40% of the sum of all the eigenvalues. Thus one

Q. J. R. Meteorol. Soc. **00**: 1–14 (2010)

DOI: 10.1002/qj

may infer that any local areas with particularly large initial perturbations in terms of dry total energy (Equation (6) but without horizontal integration) are the most sensitive domains for the forecast over the given verification domain. In Figure 7, areas of particularly large values of dry total energy associated with the particular initial perturbations thus obtained are highlighted with shading.

Ideally, the analysis requires a large number of independently perturbed forecast members. As noted in section 2, however, only six members have been independently perturbed out of the 12 perturbed members for each of the initial dates in the JMA ensemble forecast we utilize. Still, there are totally 64 $(= 2^6)$ combinations that can be formed for our sensitivity analysis by assigning the polarity (either "positive" or "negative") of the six independently perturbed members. For each of the 64 combinations, we evaluated the vertically-integrated total energy locally (based on Equation (6) without horizontal integration) by solving Equation (9) for the first eigenvector before taking their average.

As the first exercise of our sensitivity analysis, the verification time and domain were set to be 16 January and a region over the subpolar North Atlantic (310°E-340°E and 50°N-65°N), respectively. In that domain, the forecast spread for that day is largest (Figure 4(b)) in correlation with the developing blocking anticyclone. The matrix H in Equation (5) was determined to represent dry total energy integrated horizontally over the subpolar North Atlantic and vertically between the 1000- and 100-hPa levels. As shown in Figures 7(a) and 7(b), the forecasted blocking high intensity is particularly sensitive to the initial perturbations for either 11 or 12 January in the vicinity of the surface cyclone migrating eastward over the North Pacific, as discussed in the preceding sections.

The same analysis was repeated but with the matrix

H in Equation (5) determined for the entire stratospheric polar and subpolar domain (100- to 10-hPa levels and poleward of 50°N) on 28 January, when the observed PNJ was most strongly westward (Figure 1(a)). Even for the forecast period longer than two weeks (15 to 16 days in this case), the maximum sensitivity of the stratospheric forecast to the initial perturbations is found again around the cyclone over the central North Pacific (Figures 7(c) and 7(d)). In fact, our analysis in section 4 has suggested that the particular surface cyclone acted as the origin of the "downstream development" of the ensemble spread. Figures 7(c) and 7(d) suggest that observational errors around the particular cyclone is one of the factors that induce large discrepancies in the SSW prediction among the ensemble members. The maximum sensitivity over the Northwestern Pacific is consistent with Buizza and Palmer (1995), who showed that the particular region is one of the most dynamically unstable areas as indicated by singular vectors.

8   Evolution of analysis spread

In the preceding sections, we have suggested that the SSW event in January 2006 is particularly sensitive to initial errors around the cyclone over the North Pacific. In order to examine whether the large uncertainty of the initial field is owing to an unstable flow configuration around the cyclone, we used the daily circulation data derived from the AFES-LETKF experimental ensemble reanalysis (ALERA; Miyoshi and Yamane, 2007; Miyoshi *et al.* 2007; available at http://www.jamstec.go.jp/esc/afes/alera/), where data assimilation is based on Local Ensemble Transform Kalman Filter (LETKF; Hunt *et al.* 2007) performed on the AGCM for the Earth Simulator (AFES; Ohfuchi *et*

al. 2004, 2007). This reanalysis provides us with analysis and uncertainty in time-evolving flow fields in terms of spread among the ensemble members. Miyoshi *et al.* (2007) showed that the accuracy of ALERA in the troposphere is overall comparable to the NCEP/NCAR reanalysis (Kalnay *et al.* 1996) except over Antarctica and the southern ocean. Since ALERA does not assimilate satellite observations except satellite-based sea-surface wind data, it tends to be less accurate over the ocean than over land (Miyoshi and Yamane, 2007). Over maritime regions, uncertainty as measured by ALERA-based spread tends to be larger than the corresponding uncertainty in the JMA operational analysis in which radiance observations by satellites are included.

On 11 and 12 January (Figure 8), the ALERA-based spread, as a measure of uncertainty of the analysis data, over the North Pacific is maximised in the vicinity of the particular developing cyclone discussed above. This is probably because in the course of the data assimilation in ALERA, uncertainty in the six-hourly forecasts due to an unstable flow configuration associated with the developing cyclone could not be reduced due to the lack of enough free-tropospheric observations over the ocean. This result supports our hypothesis that large uncertainty in the intensity and/or the central position of the cyclone adds some difficulties to the particular SSW forecast. In fact, Figure 9 shows that the ALERA-based spread maxima identified around the cyclone translate downstream across the North Pacific as far as 120°W with speed of about 8° in longitude a day, following the migration of the particular low-pressure system. This relatively slow development of uncertainty following the particular cyclone can also be seen in the JMA ensemble forecast spread (dashed line in Figure 5(c)). Our result is consistent with Moteki *et al.*

(2007) and Inoue *et al.* (2009), who showed that ALERA-based spread develops horizontally and vertically from local domains with relatively poor observations. In Figure 9, the analysis spread almost diminishes over the North American continent, where more observations are available for ALERA than over the Pacific. This may mask the fast downstream extension of spread maxima in ALERA following the group velocity propagation of the observed wave packet (solid lines of Figures 5(a) and 5(b)). Nevertheless, the ALERA-based spread in the troposphere over the subpolar North Atlantic suddenly increases around 15 January (Figure 9), concomitant with the development of the prominent anticyclonic anomaly observed on the arrival of the wave packet from the Pacific. Correspondingly, ALERA-based spread in the stratosphere around 16 January was also maximised over the North Atlantic (not shown), in agreement with the JMA forecast spread (Figures 5 and 6).

9   Concluding remarks

Utilizing a product of the JMA monthly ensemble forecast system, we have examined the time evolution of forecast spread among the ensemble members during the development of a major SSW event observed in late January 2006. As the source of particularly large ensemble forecast spread (i.e., uncertainty in the forecast) for the SSW event, we have identified errors in the initial state in the vicinity of a synoptic-scale cyclone developing over the North Pacific about two weeks before the SSW event. In growing as forecast errors for the following several days, the initial errors are translated eastward into a blocking ridge over the subpolar Atlantic and then upward into the stratosphere to cause the large forecast spread in the PNJ deceleration. This three-dimensional propagation of

the forecast errors is associated with downstream development of synoptic-scale disturbances observed in the troposphere and then with upward propagation of a Rossby wave packet, both of which have been identified as important dynamical processes for the occurrence of the particular SSW event (NNM09). We have found the time evolution of the forecast spread to be consistent with the result of our sensitivity analysis, which shows that predictions of the SSW event and its precursory development of the tropospheric blocking ridge over the North Atlantic both tend to be particularly sensitive to local errors in the vicinity of a particular cyclone developing over the North Pacific in the initial field for the forecast. We have confirmed these results through our SVD analysis applied to the JMA ensemble forecast and our examination of the ALERA-analysed spread, whose development is similar to the JMA forecast spread.

At the time of January 2006, a set of ensemble forecast was conducted in the JMA monthly forecast system only once a week with a limited number of independent ensemble members. Furthermore, the forecast model at that time is known to suffer from a cold bias in the stratosphere. Thus more frequent ensemble forecasts with a larger ensemble size based on a less biased forecast model are needed to confirm our findings in the present study. We are planning to conduct a set of ensemble hindcast integrations for the SSW event we analysed with initial fields taken from the ALERA system.

While Mukougawa and Hirooka (2007) have suggested that improvement in SSW prediction does not necessarily yield better extended forecast of the tropospheric circulation, Mukougawa *et al.* (2009) have shown that prediction skill of the tropospheric NAM is higher when the stratospheric NAM is negative. Since those studies are, however, based only on a particular SSW event or those

only over five winters, more SSW events must be analysed to assess their influence on the predictability of the tropospheric circulation system.

Acknowledgements

References

Andrews DG, Holton JR, Leovy CB. 1987. *Middle Atmospheric Dynamics*. Academic Press, 489 pp

Anwender D, Harr PA, Jones SC. 2008. Predictability associated with the downstream impacts of the extratropical transition of tropical cyclones: case studies. *Mon. Weather Rev.* **136:** 3226–3247.

Baldwin MP, Dunkerton TJ. 1999. Propagation of the Arctic Oscillation from the stratosphere to the troposphere. *J. Geophys. Res.* **104:** 30937–30946.

Baldwin MP, Dunkerton TJ. 2001. Stratospheric harbingers of anomalous weather regimes. *Science* **294:** 581–584.

Bretherton CS, Smith C, Wallace JM. 1992. An intercomparison of methods for finding coupled patterns in climate data sets. *J. Climate* **5:** 541–560.

Q. J. R. Meteorol. Soc. **00**: 1–14 (2010)

DOI: 10.1002/qj

Buizza R, Palmer TN. 1995. The singular-vector structure of the Atmospheric global circulation. *J. Atmos. Sci.* **52:** 1434–1456.

Chang EKM. 1993. Downstream development of baroclinic waves as inferred from regression analysis. *J. Atmos. Sci.* **50:** 2038–2053.

Charlton AJ, O'Neill A, Lahoz WA, Massacand AC, Berrisford P. 2004. Sensitivity of tropospheric forecasts to stratospheric initial conditions. *Q. J. R. Meteorol. Soc.* **130:** 1771–1792.

Charlton AJ, O'Neill A, Lahoz WA, Massacand AC, Berrisford P. 2005. The impact of the stratosphere on the troposphere during the southern hemisphere stratospheric sudden warming, September 2002. *Q. J. R. Meteorol. Soc.* **131:** 2171–2188.

Enomoto T, Yamane S, Ohfuchi W. 2006. Simple sensitivity analysis using ensemble forecast. *Proceedings of 3rd workshop on mechanisms of climate variation and its predictability*, 40–43. (In Japanese).

Enomoto T, Ohfuchi W, Nakamura H, Shapiro MA. 2007. Remote effects of tropical storm Cristobal upon a cut-off cyclone over Europe in August 2002. *Meteorol. Atmos. Phys.* **96:** 29–42.

Harr PA, Anwender D, Jones SC. 2008. Predictability associated with the downstream impacts of the extratropical transition of tropical cyclones: methodology and a case study of Typhoon Nabi (2005). *Mon. Weather Rev.* **136:** 3205–3225.

Hirooka T, Ichimaru T, Mukougawa H. 2007. Predictability of stratospheric Sudden warmings as inferred from ensemble forecast data: Intercomparison of 2001/02 and 2003/04 winters. *J. Meteorol. Soc. Jpn.* **85:** 919–925.

Hoffmann RN, Kalnay E. 1983. Lagged average forecasting, an alternative to Monte Carlo forecasting. *Tellus* **35A:** 100–118.

Hunt BR, Kostelich EJ, Szunyogh I. 2007. Efficient data assimilation for spatiotemporal chaos: A local ensemble transform Kalman filter. *Physica D* **230:**, 112–126.

Inoue J, Enomoto T, Miyoshi T, Yamane S. 2009. Impact of observations from Arctic drifting buoys on the reanalysis of surface fields. *Geophys. Res. Lett.* **36:** L08501, doi:10.1029/2009GL037380.

Japan Meteorological Agency. 2002. Outline of the operational numerical weather prediction at the Japan Meteorological Agency. Appendix to WMO Numerical Weather Prediction Progress Report, Tokyo, 158 pp.

Kalnay ME, Kanamitsu M, Kistler R, Collins W, Deaven D, Gandin L, Iredell M, Saha S, White G, Woollen J, Zhu Y, Leetmaa A, Reynolds R, Chelliah M, Ebisuzaki W, Higgins W, Janowiak J, Mo KC, Ropelewski W, Wang J, Jenne R, Joseph D. 1996. The NCEP/NCAR 40-year reanalysis project. *Bull. Am. Meteorol. Soc.* **77:** 437–471.

Kalnay E. 2003. *Atmospheric Modeling, Data Assimilation and Predictability*. Cambridge University Press, pp364.

Langland RH, Shapiro MA, Gelaro R. 2002. Initial condition sensitivity and error growth in forecasts of the 25 January 2000 east coast snowstorm. *Mon. Weather Rev.* **130:** 957–974.

Limpasuvan V, Thompson DWJ, Hartmann DL. 2004. The life cycle of the Northern Hemisphere sudden warmings. *J. Climate* **17:** 2584–2596.

Manney GL, Krüger K, Pawson S, Minschwaner K, Schwartz MJ, Daffer WH, Livesey NJ, Mlynczak MG, Remsberg EE, Russell III JM, Waters JW. 2008. The evolution of the stratopause during the 2006 major warming: Satellite data and assimilated meteorological analyses. *J. Geophys. Res.* **113:** D11115, doi:10.1029/2007JD009097.

Matsuno T. 1971. Dynamical model of stratospheric sudden warming. *J. Atmos. Sci.* **28:** 1479–1494.

Miyoshi T, Yamane S. 2007. Local ensemble transform Kalman filtering with an AGCM at a T159/L48 resolution. *Mon. Weather Rev.* **135:** 3841–3861.

Miyoshi T, Yamane S, Enomoto T. 2007. The AFES-LETKF experimental ensemble reanalysis: ALERA. *Sci. Online Lett. Atmos.* **3:** 45–48.

Moteki Q, Shirooka R, Yoneyama K, Geng B, Katsumata M, Ushiyama T, Yamada H, Yasunaga K, Sato N, Kubota H, Reddy KK, Tokinaga H, Seiki A, Fujita M, Takayabu YN, Yoshizaki M, Uyeda H, Chuda T. 2007. The impact of the assimilation of dropsonde observations during PALAU2005 in ALERA, *Sci. Online Lett. Atmos.* **3:** 97–100.

Mukougawa H, Hirooka T. 2004. Predictability of stratospheric sudden warming: A case study for 1998/99 winter. *Mon. Weather Rev.* **132:** 1764–1776.

Mukougawa H, Sakai H, Hirooka T. 2005. High sensitivity to the initial condition for the prediction of sudden warming. *Geophys. Res. Lett.* **32:** L17806, doi:10.1029/2005GL022909.

Mukougawa, H., Hirooka T, Ichimaru T, and Kuroda Y. 2007. Hindcast AGCM experiments on the predictability of stratospheric sudden warming. *Nonlinear Dynamics in Geosciences.* 211-234, Springer-Verlag, doi:10.1007/978-0-387-34918-3_13.

Mukougawa H, Hirooka T. 2008. Predictability of the downward migration of the Northern Annular Mode: A case study for January 2003. *J. Meteorol. Soc. Jpn.* **85:** 861–870.

Mukougawa H, Hirooka T, Kuroda Y. 2009. Influence of stratospheric circulation on the predictability of the tropospheric Northern Annular Mode. *Geophys. Res. Lett.* **36:** L08814, doi:10.1029/2008GL037127.

Nishii K, Nakamura H, Miyasaka T. 2009. Modulations in the planetary wave field induced by upward-propagating Rossby wave packets prior to stratospheric sudden warming events: A case study. *Q. J. R. Meteorol. Soc.* **135:** 39–52

Ohfuchi W, Nakamura H, Yoshioka M, Enomoto T, Takaya K, Peng X, Yamane S, Nishimura T, Kurihara Y, Ninomiya K. 2004. 10-km mesh meso-scale resolving global simulations of the atmosphere on the

Q. J. R. Meteorol. Soc. **00**: 1–14 (2010)

DOI: 10.1002/qj

Earth Simulator: Preliminary outcomes of AFES (AGCM for the Earth Simulator). *J. Earth Simulator* **1:** 8-34.

Ohfuchi W, Sasaki H, Masumoto Y, Nakamura H. 2007. "Virtual" atmospheric and oceanic circulations in the Earth Simulator. *Bull. Am. Meteorol. Soc.* **88:** 861–866.

Onogi K, Tsutsui J, Koide H, Sakamoto M, Kobayashi S, Hatsushika H, Matsumoto T, Yamazaki N, Kamahori H, Takahashi K, Kadokura S, Wada K, Kato K, Oyama R, Ose T, Mannoji N, Taira R. 2007. The JRA-25 Reanalysis. *J. Meteorol. Soc. Jpn.* **85:** 369–432.

Plumb RA. 1985. On the three-dimentional propagation of stationary waves. *J. Atmos. Sci.* **42:** 217–229.

Rabier F, Klinker E, Hollingsworth A. 1996. Sensitivity of forecast errors to initial conditions. *Q. J. R. Meteorol. Soc.* **122:** 121–150.

Toth Z, Kalnay E. 1993. Ensemble forecasting at NMC: the generation of perturbations. *Bull. Am. Meteorol. Soc.* **74:** 2317–2330.

Wallace JM, Lim GH, Blackmon ML. 1988. Relationship between cyclone tracks, anticyclone tracks and baroclinic wave-guides. *J. Atmos. Sci.* **45:** 439–462.

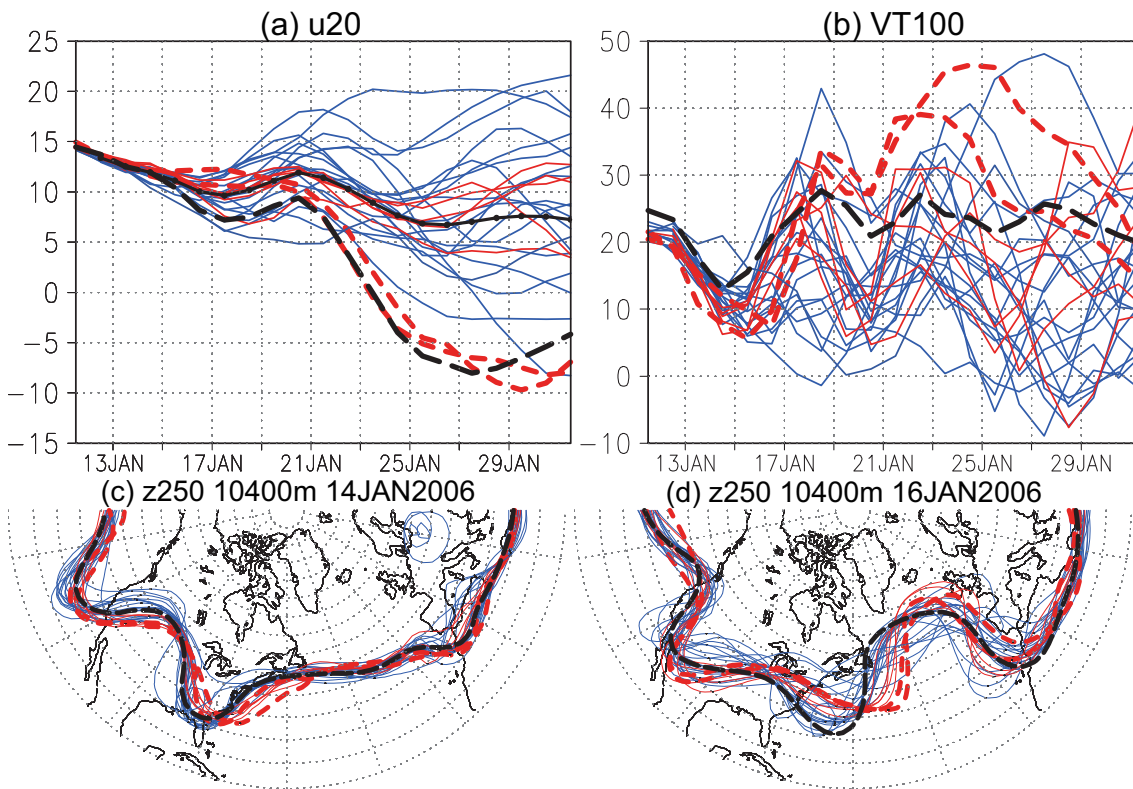Ward JH. 1963. Hierarchical grouping to optimize an objective function. *J. Am. Stat. Assoc.* **58:** 236–244.

Figure 1. (a) Time series of 20-hPa zonal-mean zonal wind (m s^{-1}) averaged over 50°N-80°N. Solid lines without any symbols denote the individual ensemble members starting on either 11 or 12 January 2006. The thick dashed line denotes observation based on the reanalysis data (JCDAS). The line with circles denotes the ensemble average, which is shown only in this panel. (b) The same as in (a), but for zonal-mean 100-hPa eddy heat flux averaged over 50°N-80°N, where eddy components of meridional wind velocity and temperature are defined as deviations from their zonal averages. (c) 10400-m isolines of 250-hPa geopotential height predicted in the individual ensemble members for 14 January (solid lines) and the corresponding observation (dashed black line). (d) The same as in (c), but for 16 January. In each panel, individual ensemble members are classified into two groups based on a cluster analysis of 250-hPa geopotential height on 14 January over the region (180°-300°E, 20°N-60°N) as shown in (c). The clusters indicated by red (cluster A) and blue (cluster B) lines include 7 and 19 members, respectively. Thick, red dashed lines in each panel highlight the two members that apparently succeeded in the prediction of PNJ deceleration in (a).
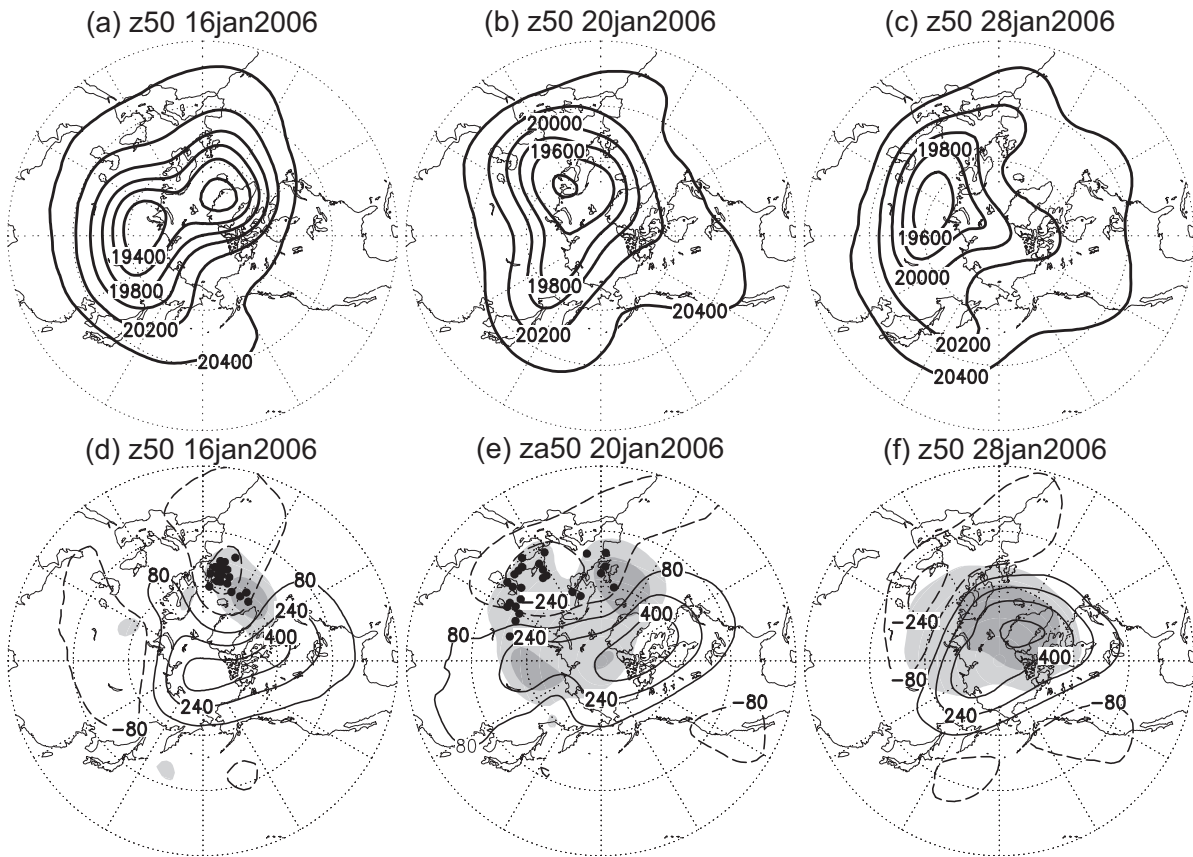
Figure 2. (a-c) 50-hPa geopotential height (contour interval; 200 m) observed on (a) 16, (b) 20 and (c) 28 January 2006. (d-f) Local spread of 50-hPa geopotential height predicted for (d) 16, (e) 20 and (f) 28 January 2006 (shaded for lightly and heavily for 0.3 - 0.6 and values greater than 0.6, respectively), superimposed on observed 50-hPa height anomalies (contoured for ±80, ±240, ±400, ±560 m; dashed for negative values). The local spread has been normalized by its instantaneous maximum within the domain poleward of $20°$N. In (d) and (e), black dots indicate the centres of 50-hPa cyclonic anomalies over Europe predicted in the individual ensemble members.

Figure 3. Zonal cross sections for $50°$N of the local ensemble spread of geopotential height predicted for (a) 16, (b) 18 and (c) 20 January 2006, shaded lightly and heavily for 0.03-0.3 and values greater than 0.3, respectively. Superimposed with contours are observed geopotential height anomalies (±30, ±90, ±150, ±210, ±270 m ; dashed for negative). At each pressure (p) level, the spread and anomaly are multiplied by $(p/1000hPa)$ and the square root of it, respectively.

(a) z250 12jan2006

(b) z250 16jan2006

(c) za250 12jan2006
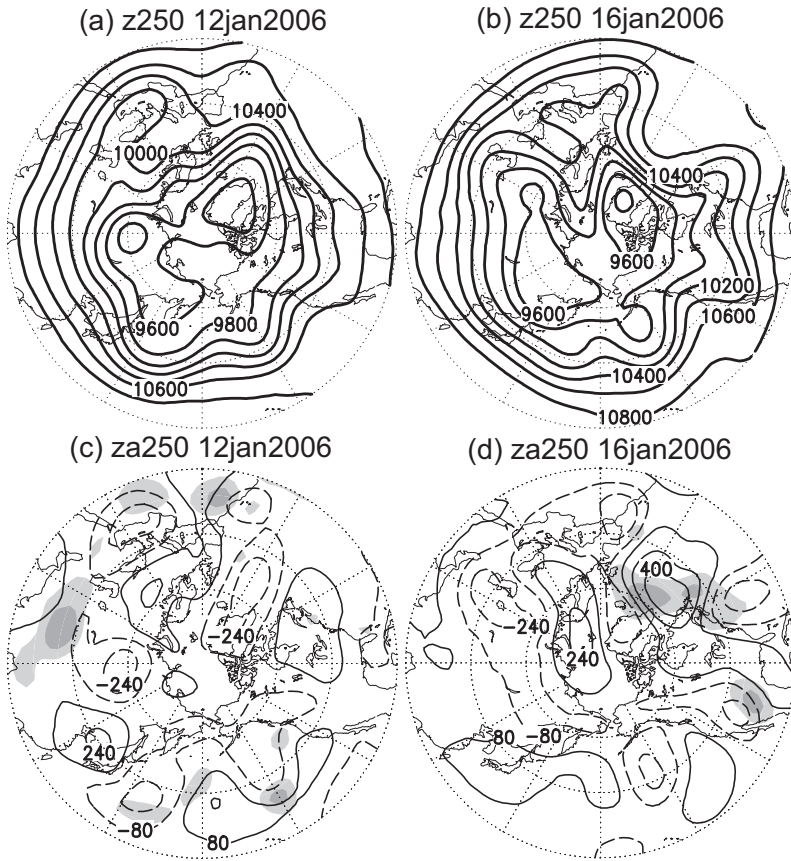
(d) za250 16jan2006

Figure 4. (a-b) As in Figure 2(a), but for 250-hPa height for (a) 12 and (b) 16 January 2006. (c-d) As in Figure 2(c), but for 250-hPa height anomaly for (c) 12 and (d) 16 January 2006.
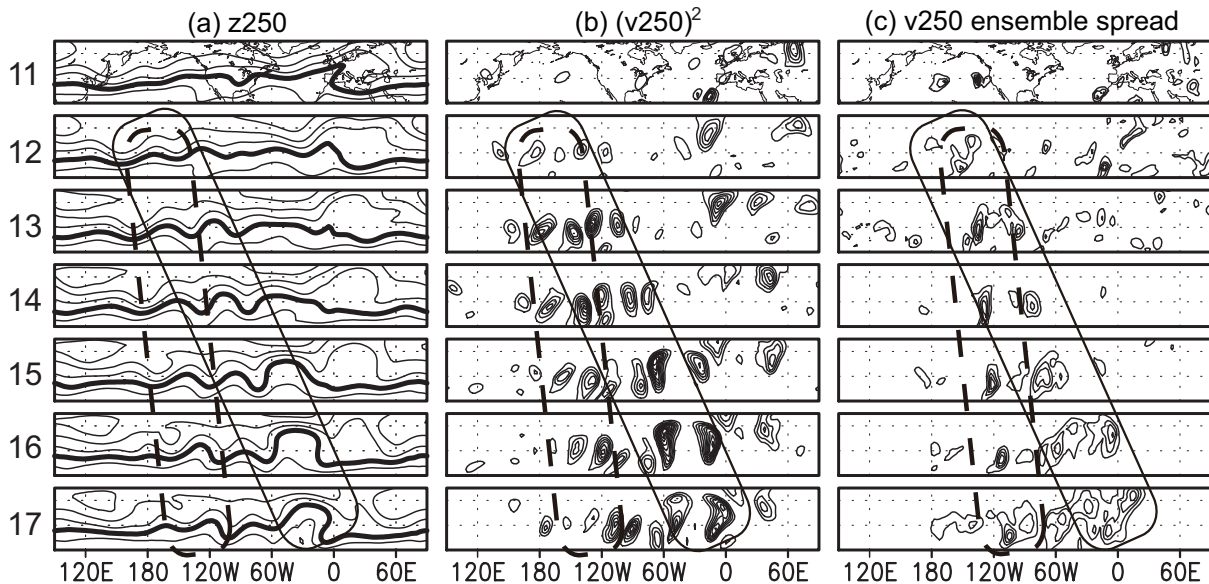
(a) z250   (b) (v250)^2 (c) v250 ensemble spread

Figure 5. (a) Time sequence of 250-hPa geopotential height observed from (top) 11 to (bottom) 17 January 2006 over a domain (20°N-70°N). Contour intervals are 300 m and the thick contour corresponds to 10400 m. (b) As in (a), but for 250-hPa meridional wind velocity squared. Contour intervals are 400 m^2 s^{-2}. (c) As in (a), but for the spread of predicted 250-hPa meridional wind velocity among the ensemble members for the initial date of 11 January. Contour intervals are 0.2. The spread has been normalized by its instantaneous maximum within the domain.
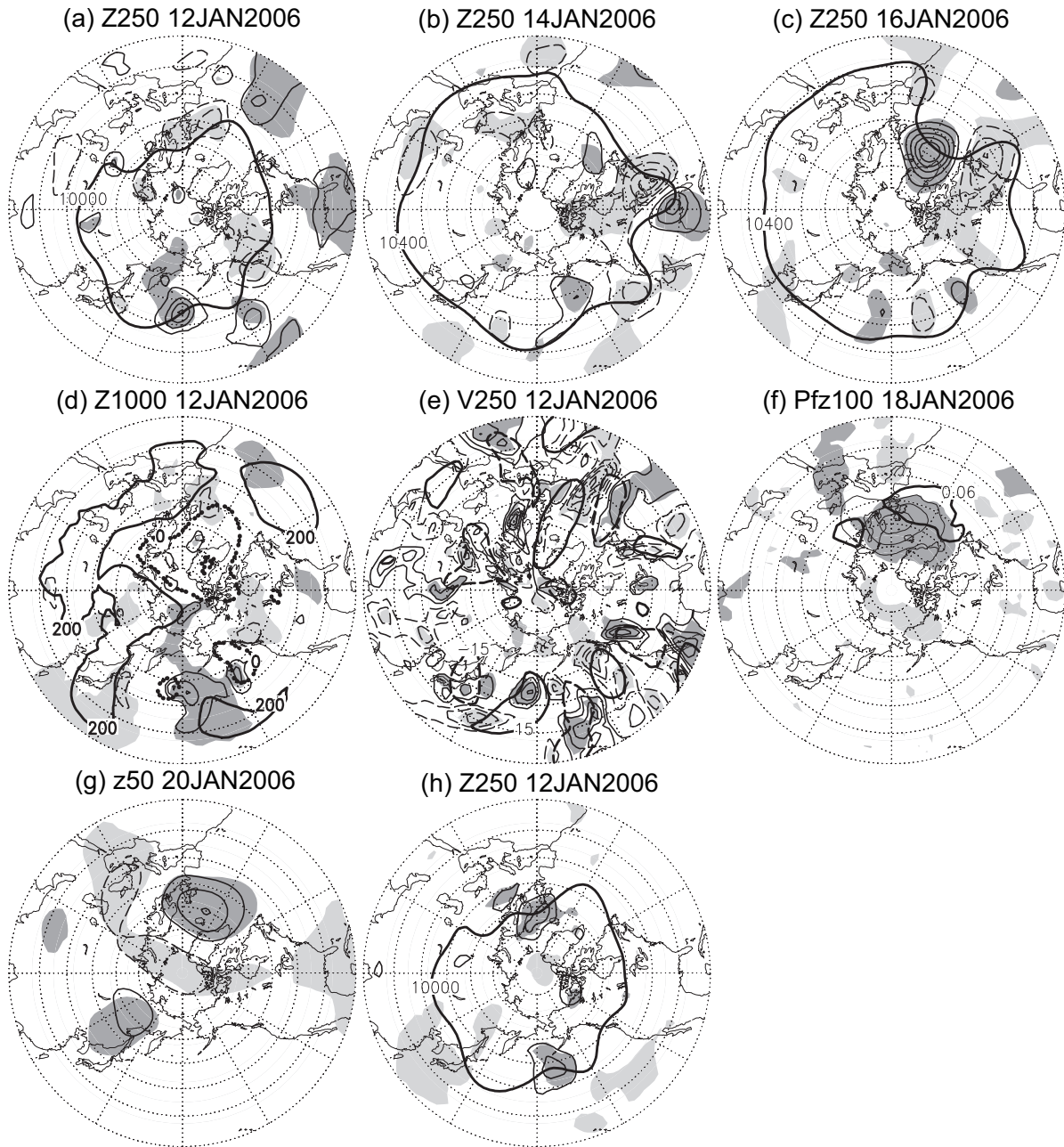
Figure 6. Results of SVD analysis based on the JMA ensemble forecasts applied to the spread of 250-hPa height over the subpolar North Atlantic forecasted for 16 January 2006 with the forecast spread of (a-c) hemispheric 250-hPa height (a) for 12 January (contour interval (CI) is 10 m and zero contours are omitted), (b) for 14 January (CI: 20 m), and (c) for 16 January (CI: 100 m). Dashed thin contours are for negative value. Heavy and light shading denotes the positive and negative correlations, respectively, whose absolute values exceed 0.4. Bold lines in (a-c) indicate specific values of 250-hPa geopotential height observed on (a) 12 (10100 m), (b) 14 (10400 m) and (c) 16 (10400m) January. (d-g) As in (a-c), but for the forecast spread of (d) 1000-hPa height for 12 January (CI: 10 m), (e) 250-hPa meridional wind for 12 January (CI: 10 m), (f) 100-hPa upward wave-activity flux for 18 January (CI: 0.01 m^2 s^{-2}) and (g) 50-hPa height for 20 January (CI: 50 m). Thick solid and dashed contours denote (d) 1000-hPa height of 200 m and 0 m, respectively, and (e) 250-hPa meridional wind velocity of 15 m s^{-1} and -15 m s^{-1}, respectively, both observed on 12 January. Thick contour in (f) denotes observed upward 100-hPa wave-activity flux of 0.06 m^2 s^{-2} for 18 January. Panels (a-g) show heterogeneous regression maps that represent typical local deviations from the ensemble mean state in an ensemble member that predicts the North Atlantic blocking stronger than the ensemble mean for 16 January. (h) As in (a) but for heterogeneous regression map of 250-hPa geopotential height (CI: 10 m) for 12 January with the normalized expansion coefficient of 50-hPa geopotential height forecasted for 28 January, based on SVD analysis applied to the hemispheric forecast spread.

(a) 11jan -> 16jan   (b) 12jan -> 16jan
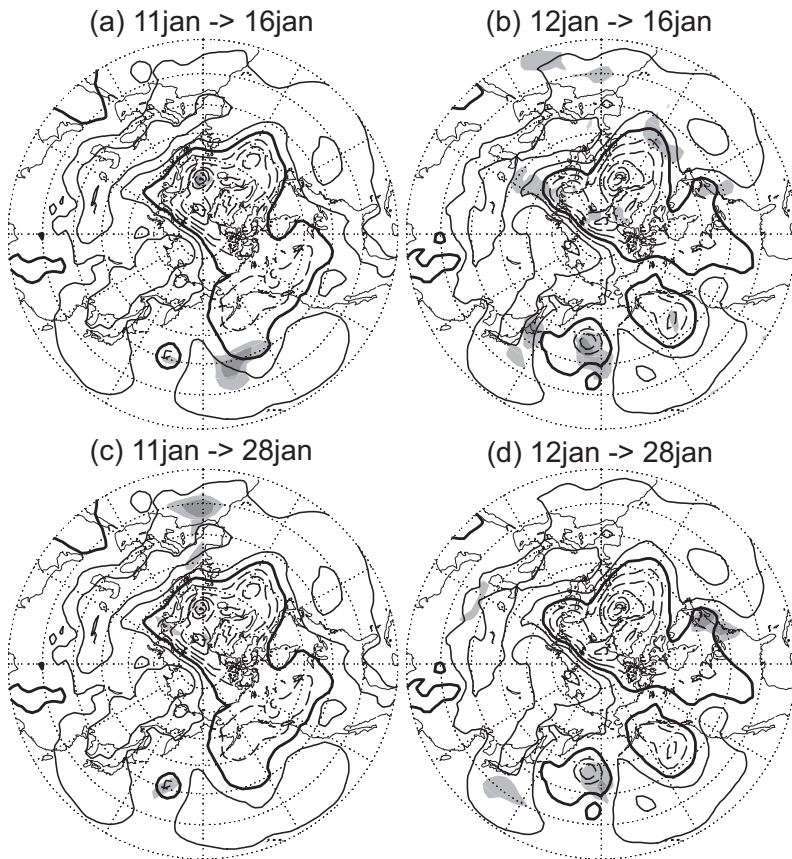### (c) 11jan -> 28jan   (d) 12jan -> 28jan

Figure 7. Results of a sensitivity analysis based on the JMA ensemble forecast. (a) Initial perturbations in the troposphere for 11 January (shaded lightly and heavily for 0.3 - 0.6 and values greater than 0.6, respectively) to which the intensity of the blocking ridge over the subpolar North Atlantic (310°E-340°E, 50°N-65°N) forecasted for 16 January is particularly sensitive. The intensities of the blocking anomaly and initial perturbations are measured as dry total energy integrated between the 1000- and 250-hPa levels and then normalized by its instantaneous maximum within the entire northern hemisphere poleward of 20°N. Superimposed with contours is sea-level pressure (every 10 hPa; dashed for less then 1010 hPa; thick solid contours for 1010 hPa) observed on 11 January. (b) Same as in (a) but initial perturbations for 12 January 2006 to which the North Atlantic blocking forecasted from 16 January is sensitive. (c-d) Same as in (a) but for initial tropospheric perturbations for (c) 11 and (d) 12 January 2006 to which lower-stratospheric (100-50hPa) field over the entire domain poleward of 50°N forecasted for 28 January is particularly sensitive.
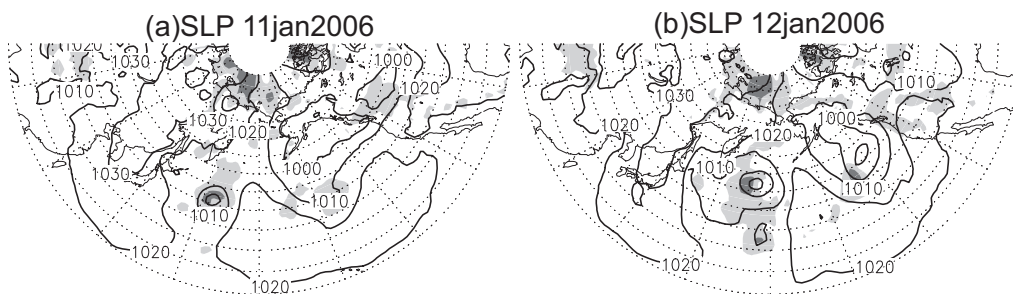
(a)SLP 11jan2006   (b)SLP 12jan2006

Figure 8. Sea-level pressure on (a) 11 and (b) 12 January 2006 produced by ALERA (contoured for every 10 hPa). Shaded lightly and heavily where the ensemble spread is between 1 and 2 [hPa] and greater than 2 [hPa], respectively.
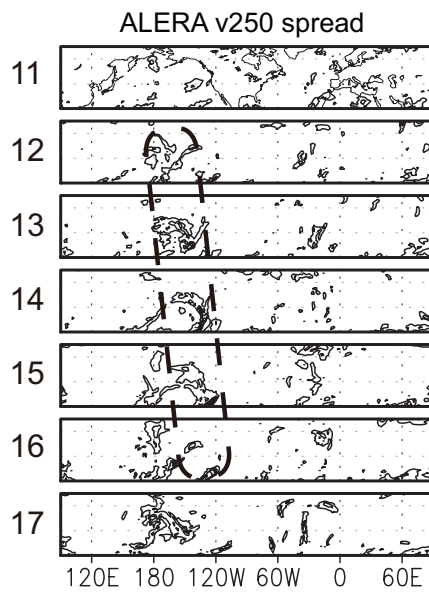
Prepared using qjrms3.cls

ALERA v250 spread

Figure 9. As in Figure 5(c), but for ALERA-based spread of 250-hPa meridional wind velocity (contoured for every 6 m^2 s^{-2}).